Hydrate-phobic Surfaces

by

Jonathan David Smith

B.S. Mechanical Engineering
University of Illinois at Urbana-Champaign, 2009

SUBMITTED TO THE DEPARTMENT OF MECHANICAL ENGINEERING IN PARTIAL
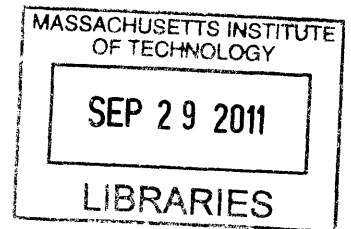FULFILLMENT OF THE REQUIREMENTS FOR THE DEGREE OF

MASTER OF SCIENCE IN MECHANICAL ENGINEERING
AT THE
MASSACHUSETTS INSTITUTE OF TECHNOLOGY

JUNE 2011

©2011 Jonathan David Smith. All rights reserved.

The author hereby grants to MIT permission to reproduce
and to distribute publicly paper and electronic
copies of this thesis document in whole or in part
in any medium now know or hereafter created.

Signature of Author: _____
Department of Mechanical Engineering
May 13, 2011

Certified by: _____
Kripa K. Varanasi
d'Arbeloff Assistant Professor of Mechanical Engineering

Accepted by: _____
David E. Hardt
Ralph E. and Eloise F. Cross Professor of Mechanical Engineering
Graduate Officer

1

Hydrate-phobic Surfaces

by

Jonathan David Smith

Submitted to the Department of Mechanical Engineering
on May 20, 2011 in Partial Fulfillment of the
Requirements for the Degree of Master of Science in
Mechanical Engineering

ABSTRACT

Clathrate hydrate formation and subsequent plugging of deep-sea oil and gas pipelines represent a significant bottleneck for ultra deep-sea production. Current methods for hydrate mitigation focus on injecting thermodynamic or kinetic inhibitors into the flow, heating the pipe walls, or managing the flow of formed hydrates. These methods are expensive and energy intensive. An alternative approach involves reducing the adhesion of hydrates to surfaces, ideally to a low enough level that the force of flow detaches them and prevents plug formation. Systematic and quantitative studies of hydrate adhesion on smooth surfaces with varying energies were conducted. Surface energies were quantified using van Oss–Chaudhury–Good analysis of advancing and receding contact angles of polar and nonpolar fluids. The strengths of hydrate adhesion to these surfaces were measured using a custom-built testing apparatus, and greater than 75% reduction in adhesion strength of Tetrahydrofuran hydrate was achieved on treated surfaces compared with bare steel. This reduction is achievable on surfaces characterized by low Lewis acid, Lewis base, and van der Waals contributions to surface free energy such that the work of adhesion is minimized. Hydrate adhesion strength was correlated with the practical work of adhesion, i.e. with $\gamma_l(1+\cos\theta_{rec})$, of a suitable probe fluid, that is, one with similar surface energy properties to those of the hydrate. These fundamental studies provide a framework for the development of hydrate-phobic surfaces, and may lead to passive enhancement of flow assurance and prevention of blockages in deep-sea oil and gas operations.

Thesis Supervisor: Kripa K. Varanasi

Title: Assistant Professor of Mechanical Engineering

Introduction

The most recent world energy outlook predicts that energy demand in 2035 will be 36% higher than in 2008[1]. The Department of Energy and The Oil and Gas industry are looking at ultra deep-sea exploration as a next frontier for meeting these increasing global energy needs. However, many challenges need to be overcome before drilling and production at greater depths becomes economical. One pressing challenge is the formation of natural gas hydrates in oil and gas pipelines. Hydrates are crystalline structures formed by a lattice of water cages, entrapping hydrocarbon molecules elevated pressures and low temperatures[2]. Hydrates can plug oil lines, forcing operations to stop until they are removed, and in some extreme events, can pose safety issues by being a projectile within the line if subjected to pressure differentials[3] Flow assurance is a major challenge and represents a significant bottleneck for ultra deep-sea exploration. Current methods for hydrate mitigation focus on the use of chemicals to shift the equilibrium hydrate formation curve to higher pressures and lower temperatures, using kinetic inhibitors to slow the growth of hydrates, and insulating or heating the pipeline walls.[4-6] The costs associated with these methods and with lost oil and gas production due to hydrate plugging can run into billions of dollars (more than $200 M USD is spent annually just on hydrate inhibiting chemicals[3]). Furthermore, these methods are energy intensive and environmentally unfriendly, and alternative approaches to reduce hydrate adhesion are of great interest.

In this paper, we study a new approach for preventing hydrate plug formation: reducing hydrate adhesion strength to the pipeline wall. We develop a fundamental understanding of hydrate adhesion as a function of surface energy properties and provide tools for straightforward design of hydrate-phobic surfaces. The approaches laid out in this paper could provide a pathway to enhance flow assurance and enable oil and gas production from ultra-deep sea reserves.

While hydrate nucleation and formation have been described in the literature[6-15], there are relatively few studies on hydrate adhesion. Most adhesion studies to date have used a micromechanical adhesion testing apparatus to measure adhesion forces between hydrate particles, or between hydrate and ice particles[16-19]. A few investigations have examined the effect of surface wettability on capillary forces between hydrate particles and surfaces[20, 21]. These studies concluded that the deposition of hydrate particles from the fluid bulk onto the pipeline wall is unlikely, because the capillary forces involved are insufficient to maintain adherence of the hydrate particles under flow conditions. However, much higher adhesion forces were reported for hydrates that were grown directly on a surface, indicating that hydrates that form on pipeline walls would likely remain adhered under the force of the flow and providing evidence that their adhesion is governed by forces other than capillary forces. The effect of wettability and surface energy on the adhesion strength of gas hydrates that form directly on a surface has not been explored. In this paper we systematically investigate the effect of wettability and surface energy on hydrate adhesion strength.

This work was inspired by numerous studies of the relationships between water wettability and ice adhesion strength that were summarized in detail by Meuler et al[22] and are briefly described here. Petrenko and Whitworth compiled ice adhesion strength and water contact angle data from several groups on a single plot and found that while ice adhesion strength generally decreased with increasing water contact angle, significant scatter was present in the data[23]. Meuler et al[24] expanded upon this work by investigating relationships between ice adhesion strength and various measures of water wettability on surfaces with varying chemistry. They reported a strong linear correlation between the work of adhesion for liquid water that is calculated from receding contact angles (i.e. $W_{water,rec}^{a} = \gamma_{water}(1 + \cos\theta_{rec})$, the practical work of

4

adhesion) and ice adhesion strength. Furthermore this correlation passed through the origin, suggesting that the water parameter $(1 + \cos\theta_{rec})$ is physically meaningful for ice adhesion. The importance of this result is that simple measurements of receding contact angles become a powerful tool for the design of ice-phobic surfaces.

Here we follow the methodology of Meuler et al and measure THF hydrate adhesion strength on surfaces with a range of wettabilities. Hydrate adhesion strength decreases with surface energy and can be predicted using the work of adhesion of a suitable probe fluid. These studies provide valuable insights into the design of hydrate-phobic surfaces.

Experiment

Adhesion testing methodology

Tetrahydrofuran (THF) hydrate is used as a model system because THF is completely miscible in water and forms hydrate at atmospheric pressure and temperatures below 4.4 °C for a solution of 19.1% THF (by weight) in water[2]. The adhesion testing setup and protocol used in this work is shown schematically in Figure 1. A solution of 19.1 wt.% THF in deionized (DI) water was poured into glass cuvettes that were frozen to the test substrates. The substrates were first clamped down on a custom-built base plate (4 x 5 array). The 19.1 wt. % THF/water solution (1.5 mL) was syringed into 20 glass cuvettes (1 cm x 1 cm x 4.4 cm, Scientific Equipment of Houston) that had been modified by: (1) polishing the tops of the open ends using a Buehler EcoMet 250/300 Grinder-Polisher equipped with 1200 grit; (2) treating the cuvettes with trichloro (1H, 1H, 2H, 2H-perfluoroctyl) silane vapor to reduce their surface energies. These modified cuvettes were then loaded into a home-built sample holder (4 x 5 array). The base plate was inverted and placed on top of the sample holder, and this assembly was bolted together to provide flush contact between the cuvettes and test substrates. The THF/water solution typically

did not leak from the inverted cuvettes, provided the glass had been polished to enhance the physical contact with the test substrate and treated with trichloro (1H, 1H, 2H, 2H-perfluoroctyl) silane to reduce its surface energy and wettability. This assembly was mounted on top of a liquid-cooled Peltier cooling plate (TECA Corporation, model LHP-800CP) that was housed in a nitrogen atmosphere with relative humidity below 5% to minimize frost formation on the samples and test apparatus. Before freezing the samples, the sample holder was carefully removed. The liquid columns were then frozen for 2 hours at -15°C (the substrate temperature was monitored using a thermocouple attached to the top of one of the substrates) to yield hydrate columns encased in cuvettes and adhered to the test substrates.
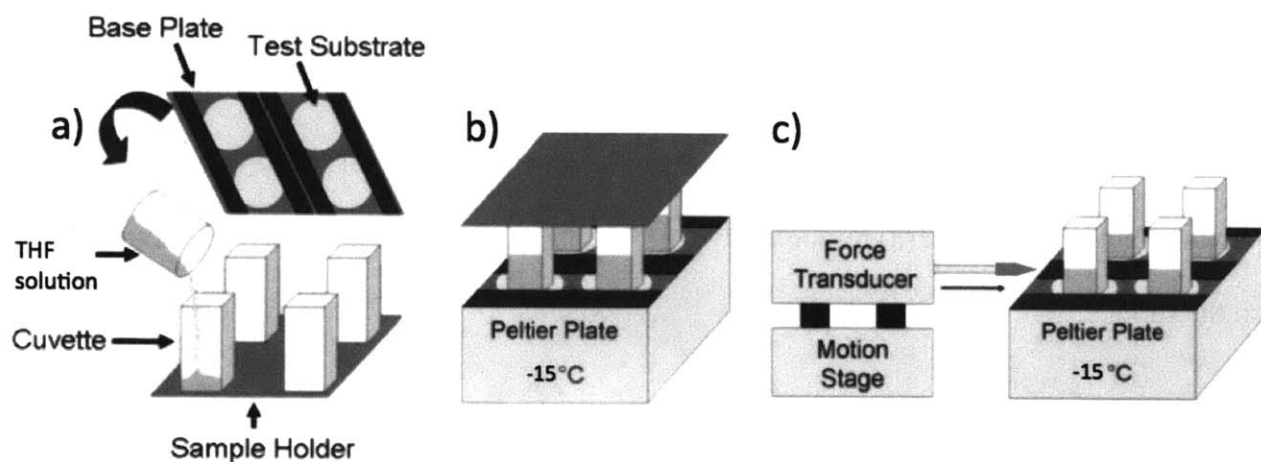

Figure 1. Schematic depiction of the procedure used to freeze hydrate columns on test substrates and to measure the hydrate adhesion strength. The actual apparatus can hold a 4 x 5 array of samples; a 2 x 2 array is used here for ease of illustration. (a) A 19.1 wt. % solution of THF in DI water is poured into cuvettes housed in a sample holder (bottom) and the test substrates are clamped onto a base plate (top). The samples attached to the base plate are then mounted flush against the tops of the cuvettes. (b) The base plate-sample holder assembly is taken into a glove box operating under a nitrogen atmosphere, inverted, and bolted to a Peltier cooling plate whose surface is thermostated at -15 °C. The top sample holder is then removed and an insulating foam box is placed over the assembly to reduce the cooling load required of the chiller and the hydrate columns are allowed to freeze for two hours. (c) The insulating box is removed and the wedge-shaped probe of a force transducer is propelled at 1mm/s into the side of each cuvette at a height of 9.3mm until the hydrate detaches from the test surface. The maximum force is recorded and converted into hydrate adhesion strength using the known cross-sectional area of the hydrate-substrate interface.

The force required to detach each hydrate column from its test substrate was measured by driving a 12mm wide wedge-shaped probe head of a force transducer (Imada, model ZP–44) into contact with the side of the hydrate-filled cuvette at a constant velocity of 1 mm/s and continuing to drive the probe forward until the hydrate breaks free from substrate. The probe velocity was controlled using a motion stage (MICOS, model VT80). The sharp edge of the probe head was located 9.3 mm above the substrate. Hydrate adhesion strength was obtained by dividing the measured maximum force with the known cross-sectional area (1 cm^2) of the hydrate-substrate interface.

A photograph of the test apparatus is provided in Figure 2(a). Side view photographs of the base of the cuvettes were taken as the THF/water mixture was subcooled during the hydrate freezing process to demonstrate the mechanism of hydrate formation (Figures 2(b) through 2(f)) . The hydrate forms on the surface, which is at the lowest temperature, (figure 2(c)) and grows into the solution (Figures 2(d) through 2(f)), confirming that heterogeneous nucleation occurred on the surface.
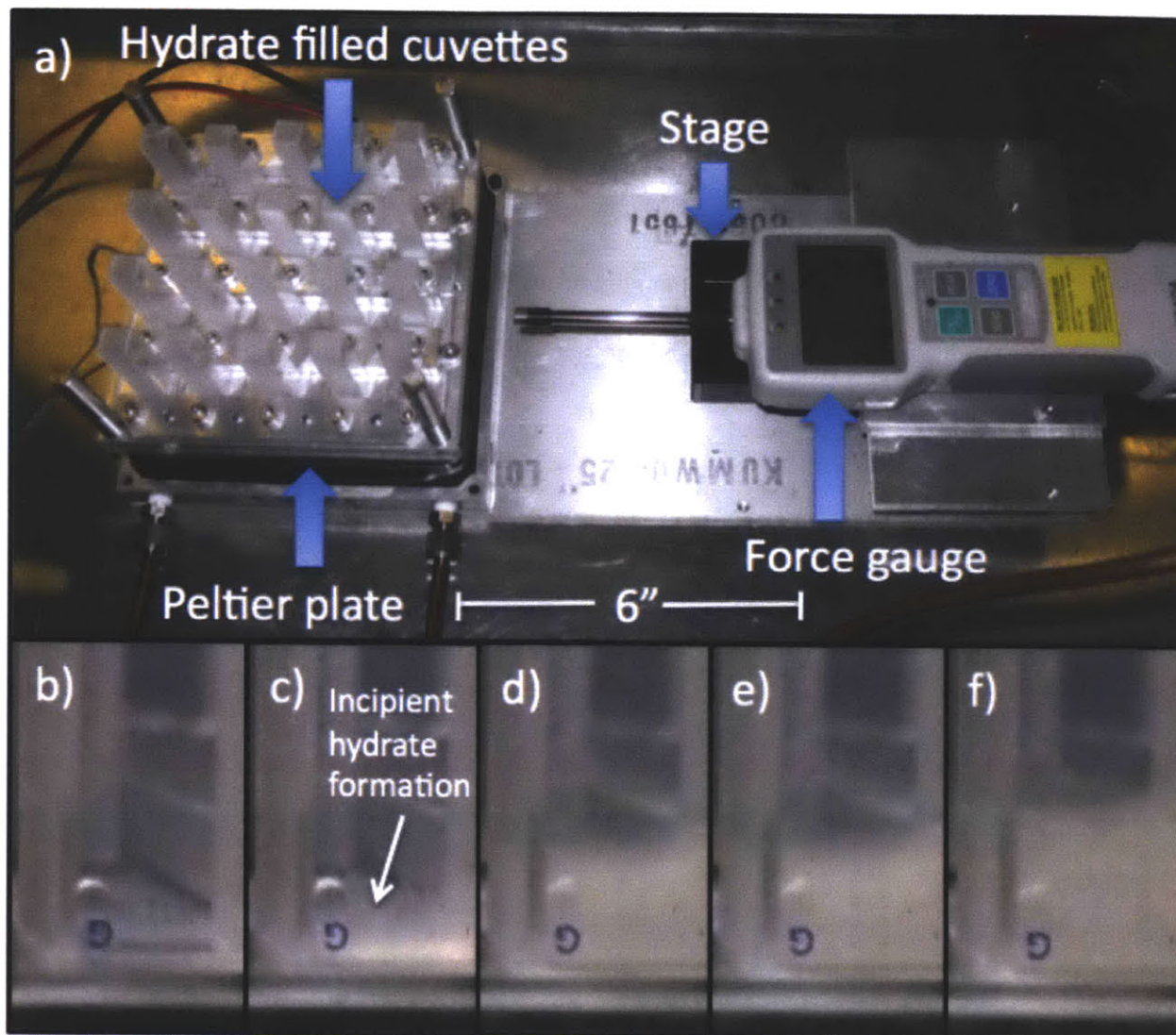
Figure 2. Photograph of the test apparatus and side view photographs of the base of the cuvettes taken during the hydrate freezing process on a trichloro (1H, 1H, 2H, 2H-perfluoroctyl) silane-treated substrate b) sub-cooled THF/water mixture before the onset of hydrate formation c) The THF hydrate begins to grow from the substrate surface, confirming that heterogeneous nucleation occurred at the solution-substrate interface. Hydrate growth continues (d-f) until the columns of solution are completely solidified.

Substrate selection and preparation

A library of test surfaces with varying chemistry was established in order to elucidate the influence of surface properties, such as wettability and surface energy, on adhesion strength. These surfaces, ranging from hydrophilic to hydrophobic, include thiolated gold, silane-treated

glass, and a blend of 80%/20% PEMA/fluorodecyl polyhedral oligomericsilsesquioxane (fluorodecyl POSS)[25] spin coated onto steel. Surface energies of each of the test substrates were calculated obtained van Oss–Chaudbury–Good (vOCG) analysis[26] from measured advancing and receding contact angles of up to 6 probe fluids (described in the following section), Advancing and receding contact angles of DI water and surface energies calculated from advancing contact angles of the probe fluids are provided in Figure 3 for each of the surfaces tested.
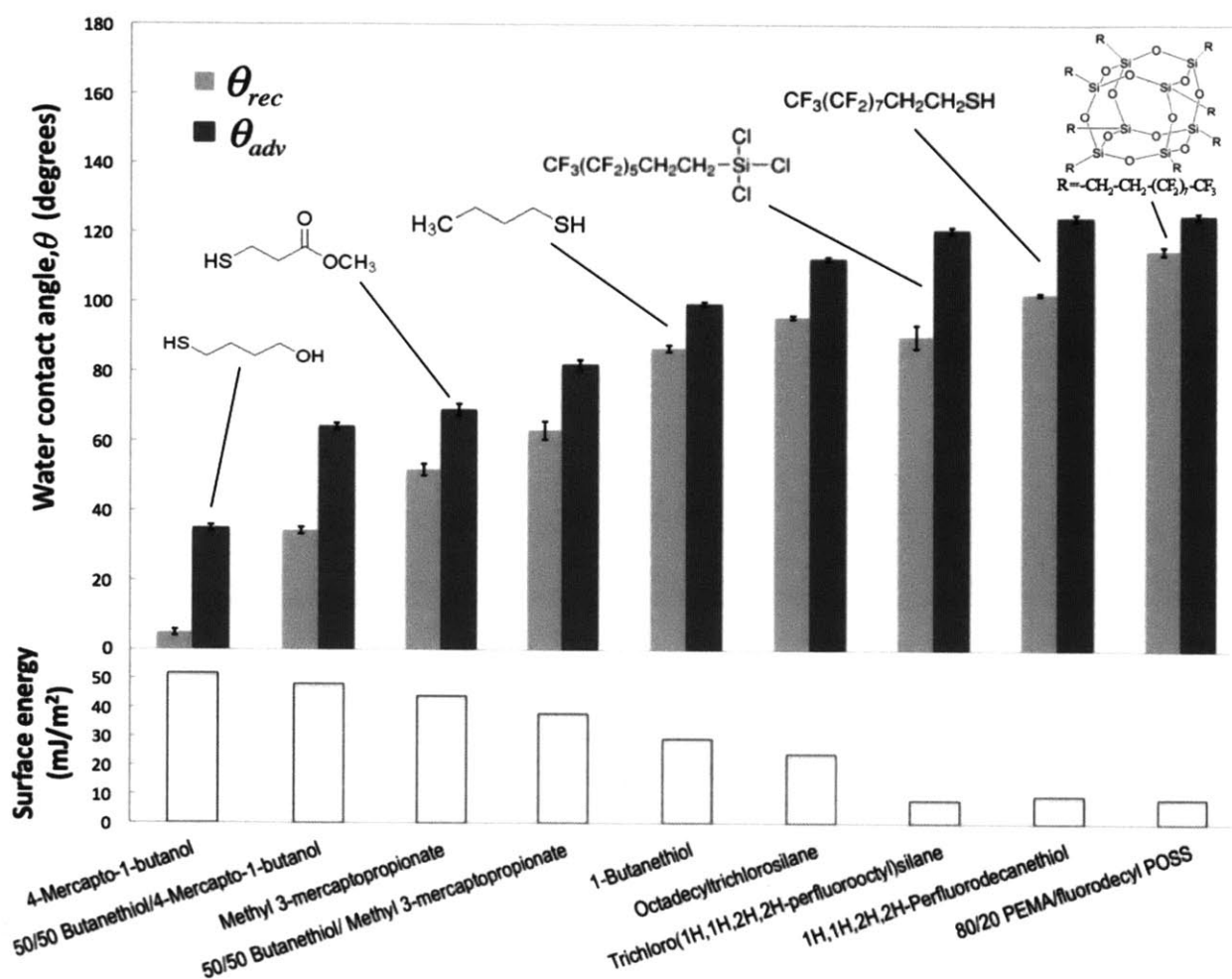

Figure 3: Advancing and receding contact angle measurements of DI water on each of the test substrates (top). Surface energies of each of the of the test calculated using vOCG analysis of measured advancing contact angles of polar and nonpolar probe fluids (bottom). Advancing contact angles range from 35° to 125° and receding contact angles range from 5° to 115° Surface energies range from 8 mJ/m² to 52 mJ/m².

Thiol compounds were purchased from Sigma-Aldrich based on the hydrophobic, hydrophilic and Lewis acid-Lewis base properties of the terminal groups. A 1mM solution of each thiol was prepared using 100% pure ethanol as the solvent. Evaporated gold-coated glass slides, 100nm in thickness (with a 5nm intermediate layer of titanium), were purchased from Evaporated Metal Films. Prior to adhesion and contact angle measurements, the slides were rinsed with ethanol and then placed in the thiol solutions for at least 24 h. The slides were then removed from the solutions, rinsed again with ethanol and dried with nitrogen immediately before the measurements. The slides were never exposed to air for longer than 10 min to minimize degradation[27]. After contact angle measurements the slides were rinsed with ethanol again and returned to their 1mM thiol solution to prevent degradation.

Glass slides, from VWR, were cleaned by the following protocol: (i) sonication first in a 4% by volume solution of Micro-90 detergent (International Products Corporation) in DI water for 15s, (ii) sonication in water for 15min, repeated twice, (iii) rinsing with water between sonications to ensure complete removal of the Micro-90. The cleaned slides were then either stored in DI water until adhesion testing, or they were plasma cleaned and treated with octadecyltrichlorosilane (Sigma Aldrich) by solution deposition or with trichloro (1H, 1H, 2H, 2H-perfluoroctyl) silane (Sigma Aldrich) by vapor deposition in a dessicator at vacuum pressure of -26.5 inHg for 3hr.

Steel discs, purchased from Marv-o-lus Manufacturing, were cleaned by scrubbing with acetone and then stored in acetone overnight. The cleaned steel discs were tested directly, or a

blend of 80%/20% PEMA/fluorodecyl POSS was deposited on them with a spin-coater prior to testing.

Contact angle measurements

Contact angles of four polar fluids: DI water (18 MΩ-cm, Millipore), ethylene glycol (Alfa Aesar) and formamide (Alfa Aesar), and a 19.1 wt.% mixture of THF (Alfa Aesar) in DI water, and two nonpolar fluids: alphabromonaphthalene (Alfa Aesar) and diiodomethane (Alfa Aesar), were measured on the test surfaces using a ramé-hart Model 500 Advanced Goniometer/ Tensiometer. Advancing (θ_{adv}) and receding (θ_{rec}) angles were measured for each fluid as they were supplied via a syringe into or out of sessile droplets (drop volume ~5 μL) at a rate of 0.2 μl/s, yielding contact line velocities less than 1 mm/min. The resulting capillary numbers ($Ca = \mu V / \gamma$) were less than 10^{-5} for all fluids tested, ensuring that the measured dynamic contact angles were essentially the same as contact angles obtained immediately after the contact line comes to a stop[28-31]. Advancing and receding surface energies were computed using vOCG analysis[26] of the gathered advancing and receding contact angle data. The Lifshitz-van der Waals, Lewis acid, and Lewis base parameters of surface tensions, as well as the total surface tensions (γ^{LW}, γ^{+}, γ^{-}, and γ respectively) are provided in Table 1. Different values are obtained depending on whether advancing or receding values of probe fluids are used in the vOCG analysis. Some "receding surface energies" could not be determined because non-zero receding contact angles of at least one nonpolar and two polar probe fluids were not always attained.

Table 1. Surface energy properties of the tested substrates, calculated from advancing and receding contact angles of DI water, ethylene glycol, formamide, alphabromonaphthalene, and diiodomethane using vOCG analysis, where $\gamma^{total} = \gamma^{LW} + 2\sqrt{\gamma^+}\sqrt{\gamma^-}$

Substrate	Advancing surface energy data				Receding surface energy data			
	γ^{LW} (mJ/m²)	$\sqrt{\gamma^+}$ (mJ$^{1/2}$/m)	$\sqrt{\gamma^-}$ (mJ$^{1/2}$/m)	γ^{total} (mJ/m²)	$\sqrt{\gamma^{LW}}$ (mJ$^{1/2}$/m)	$\sqrt{\gamma^+}$ (mJ$^{1/2}$/m)	$\sqrt{\gamma^-}$ (mJ$^{1/2}$/m)	γ^{total} (mJ/m²)
1-Butanethiol	31.5	-0.6	1.5	29.2	41.7	-0.3	1.9	39.8
1H,1H,2H,2H-Perfluorodecanethiol	9.8	0.5	-0.2	9.6	25.2	-0.3	1.4	24.1
Methyl 3-mercaptopropionate	44.6	-0.1	3.7	43.9	47.5	0.4	4.9	51.7
4-Mercapto-1-butanol	45.6	0.5	6.4	51.7	N/A	N/A	N/A	N/A
50/50 Butanethiol/ Methyl 3-mercaptopropionate	40.3	-0.4	2.8	37.9	47.2	-0.2	4.3	44.7
50/50 Butanethiol/4-Mercapto-1-butanol	44.5	0.5	3.7	48.1	50.6	0.3	6.3	54.4
Trichloro (1H,1H,2H,2H-perfluorooctyl)silane	7.6	0.8	0.3	8.0	24.9	0.1	2.4	24.5
Octadecyltrichlorosilane	24.4	-0.3	0.2	24.0	30.0	-0.4	1.9	28.0
80/20 PEMA/fluorodecyl POSS	8.7	0.1	0.3	8.6	12.3	-0.2	1.1	11.7
Clean glass	40.8	0.7	7.8	51.1	N/A	N/A	N/A	N/A
Bare steel	39.1	-0.3	3.9	36.4	N/A	N/A	N/A	N/A

The surface tension, and therefore the contact angle, of the THF/water solution varies with time due to evaporation of THF from the solution. The variation of surface tension with time was measured using the pendant drop method[32]. Based on these measurements, care was taken to measure advancing and receding contact angles of the THF/water solution before significant evaporation of THF from the solution could occur.

Surface roughness characterization

Surface texture plays an important role in adhesion and can often result in interlocking of the adhering materials. This was demonstrated recently in our prior studies of ice adhesion studies, in which we observed an linear increase in adhesion strength with the Wenzel roughness, that is, the total surface area divided by the occluded area[33]. For the purpose of this study, we are interested in studying the effects of surface chemistry alone, and therefore focus on smooth surfaces. Surface profilometry was conducted to verify the smoothness of our test surfaces. A Tencor P-12 profilometer with a 2um radius stylus and a Zygo interferometer were used to measure the roughness of the steel disc and the 80%/20% PEMA/fluorodecyl POSS coated steel disc. Atomic force microscopy (AFM) was carried out on glass, gold, and some representative silanes and thiols using a VeecoDimension 3100 scanning probe microscope operating in the tapping mode. The measured roughness data are provided in Table 2. The Wenzel roughness is r < 1.06 for all surfaces tested.

Table 2: Roughness data for some representative silanes and thiols. The Wenzel roughness (total surface area/ occluded area) is r < 1.06 for all surfaces tested.

Substrate	Root-Mean Square Roughness, R_q	Wenzel Roughness, r
Clean glass	0.63 ± 0.1 nm	1.01
Trichloro (1H,1H,2H,2H-perfluorooctyl)silane	1.82 ± 0.07 nm	1.06
Gold	2.06 ± 0.07 nm	1.04
1H,1H,2H,2H-Perfluorodecanethiol	2.30 ± 0.07 nm	1.03
Bare steel	0.85± 0.04μm	1.01
80/20 PEMA/fluorodecyl POSS	0.85 ± 0.04μm	1.01

Results and discussion

Results of the adhesion tests for all test surfaces are shown in Table 3 along with calculated

advancing and receding surface energy data. A ~75% reduction in adhesion strength was

observed on some surface chemistries compared to bare steel, and in general, the adhesion

strength decreases with the substrate surface energy. These results demonstrate the importance of

surface chemistry to adhesion strength. However, to design surfaces for reduced adhesion, the

key surface properties that affect adhesion must be determined.

Table 3. Measured hydrate adhesion strength, number of adhesion tests, and advancing and
receding surface energies calculated for each test surface.

Substrate	THF hydrate adhesion strength (kPa)	Number of tests	Total surface energy (mJ/m^2)	
	τ_h		γ_{adv}	γ_{rec}
Bare steel	402 ± 150	8	36.4	NA
Clean glass	283 ± 82	9	51.1	NA
4-Mercapto-1-butanol	185 ± 39	12	51.7	NA
50/50 1-Butanethiol/ 4-Mercapto-1-butanol	179 ± 45	18	48.1	NA
Methyl 3-mercaptopropionate	160 ± 32	11	43.9	51.7
50/50 Butanethiol/Methyl 3-mercaptopropionate	149 ± 20	13	37.9	44.7
Trichloro (1H,1H,2H,2H-perfluorooctyl) silane	133 ± 15	11	8.0	24.5
1-Butanethiol	121 ± 48	13	29.2	39.8
Octadecyltrichlorosilane	114 ± 23	8	24.0	28.0
1H,1H,2H,2H-Perfluorodecanethiol	111 ± 24	8	9.6	24.1
80/20 PEMA/fluorodecyl POSS	90 ± 16	11	8.6	11.7

The adhesion strength between two smooth bodies is known to depend strongly on van der Waals (apolar), electron acceptor (Lewis acid), and electron donor (Lewis base) interactions[26]. The latter interactions are generally alluded to as *polar* interactions and arise primarily due to hydrogen bonding. These interactions are therefore especially important when considering polar materials such as water, ice, or hydrates[34]. The sum of these interactions can be characterized by the thermodynamic work of adhesion, W^a, which is a function of the Lifshitz van der Waals, Lewis acid, and Lewis base parameters of surface energy of the adhering materials, denoted by γ^{LW}, γ^+, and γ^-, respectively. The work of adhesion of a material A to a material B is given by[26]

$$W_{AB}^a = 2\left(\sqrt{\gamma_A^{LW}\gamma_B^{LW}} + \sqrt{\gamma_A^+\gamma_B^-} + \sqrt{\gamma_A^-\gamma_B^+}\right) \tag{1}$$

where the subscripts A and B denote the two adhering materials.

Note that the work of adhesion of material A to itself is simply the work of cohesion of material A, W_A^c. Then by reducing the right side of Eq. 1, with both subscripts denoting material A, we obtain,

$$W_A^c = 2\left(\gamma_A^{LW} + 2\sqrt{\gamma_A^+\gamma_A^-}\right) = 2\gamma_A^{total} \tag{2}$$

Where γ_A^{total} is the total surface tension of material A.

If one of the materials (A) in Eq. 1 is a liquid that exhibits a non-zero contact angle, θ_{AB}, then the work of adhesion is also given by the Young-Dupré equation[35]:

$$W_{AB}^a = \gamma_A(1 + \cos\theta_{AB}) \tag{3}$$

Where γ_A is the total surface energy of material A. If $\theta_{AB} = 0$, then $W_{AB}^a \geq \gamma_A(1 + \cos\theta_{AB}) = 2\gamma_A$

The theory of brittle cohesive fracture published by Griffith in 1920 proposed that the cohesive strength of a brittle material, that is, the critical stress required to initiate cohesive fracture, is a function of the thermodynamic work of cohesion (Eq. 3) [36]. Griffith's fracture criterion was later extended to adhesive fracture with plastic deformation of the adhering materials, showing that adhesion strength is a function of the thermodynamic work of adhesion[37-39]. Accordingly, it is expected to have a correlation between the thermodynamic work of adhesion of two materials and their adhesion strength.

The surface energy parameters, required to calculate the work of adhesion between two solids (Eq. 1), cannot be readily determined for THF hydrate due to the rapid evaporation of THF from the hydrate surface prior to contact angle measurements. Further difficulties arise in selecting probe fluids that remain solid at temperatures below 4.4°C and insoluble in THF. Hence having a probe fluid that can be used to predict adhesion strength of the THF hydrate is desirable. For example, in studies of ice adhesion, liquid water is used as a probe fluid. Specifically, correlations are made between the adhesion strength of *ice* on a selected substrate and the work of adhesion of *liquid water* on that same substrate, though a fundamental basis for this approach has not been established.

In order to apply a similar approach to predicting hydrate adhesion, we digress here and study ice and water as a model system to provide support for a probe fluid approach and to gain insights into the selection of an appropriate probe fluid for hydrates. As discussed previously, the adhesion strength of a material to a substrate is a function of its thermodynamic work of adhesion to that substrate. However, for studies of ice adhesion, the work of adhesion of *liquid water* on a selected substrate is correlated with the adhesion strength of *ice* on that same substrate. Here we hypothesize that the existence of this correlation is attributable to the

similarity of the surface energy parameters of ice and liquid water. For water at 25°C,

$$\sqrt{\gamma^{LS}} = 4.67 \text{ mJ}^{1/2}/\text{m}, \sqrt{\gamma^+} = 5.05 \text{ mJ}^{1/2}/\text{m}, \sqrt{\gamma^-} = 5.05 \text{ mJ}^{1/2}/\text{m}, \text{and } \gamma = 72.8 \text{ mJ/m}^2, \text{and for ice}$$

at 0°C, $\sqrt{\gamma^{LW}} = 5.44 \text{ mJ}^{1/2}/\text{m}, \sqrt{\gamma^+} = 3.74 \text{ mJ}^{1/2}/\text{m}, \sqrt{\gamma^-} = 5.29 \text{ mJ}^{1/2}/\text{m}, \text{and } \gamma = 69.2$

mJ/m^2[40]. Consequently, the work of adhesion of liquid water to most materials is

approximately equal to that of ice according to Eq 1.

The near-equality between the work of adhesion of liquid water and that of ice is

demonstrated by calculating the work of adhesion of liquid water and that of ice to the surfaces

tested in this work. Using Eq. 1, the work of adhesion of ice is calculated using the surface

energy parameters of ice listed above and the surface energy parameters calculated for each of

the substrates using vOCG analysis (Table 1). The resulting values are plotted against the work

of adhesion for water, determined from its advancing and receding contact angles on the

substrates tested (Figure 5). The strong linear correlation ($R^2 = 0.99$) suggests that work of

adhesion measurements for liquid water are a good approximation of the work of adhesion of ice.

According to fracture mechanics theory, adhesion strength of ice is a function of the work of

adhesion of ice[37-39]. Consistent with this theory and the near-equality between the works of

adhesion of water and ice, the adhesion strength of ice should therefore correlate with the work

of adhesion of liquid water. That is, $\tau_{ice} = f(W_{ice}^a) \cong g(W_{water}^a)$, where τ_{ice} is the strength of ice

adhesion, W_{ice}^a is the work of adhesion of ice, and W_{water}^a is the work of adhesion of liquid water.

Different values for work of adhesion can be determined depending on the contact angle

(advancing, receding, static), used in Eq. 3. Meuler et al[24] have concluded that ice adhesion

strength correlates most strongly with the work of adhesion calculated from receding contact

angle measurements, $\gamma_{water}(1 + \cos\theta_{rec})$, that is, with the practical work of adhesion for liquid
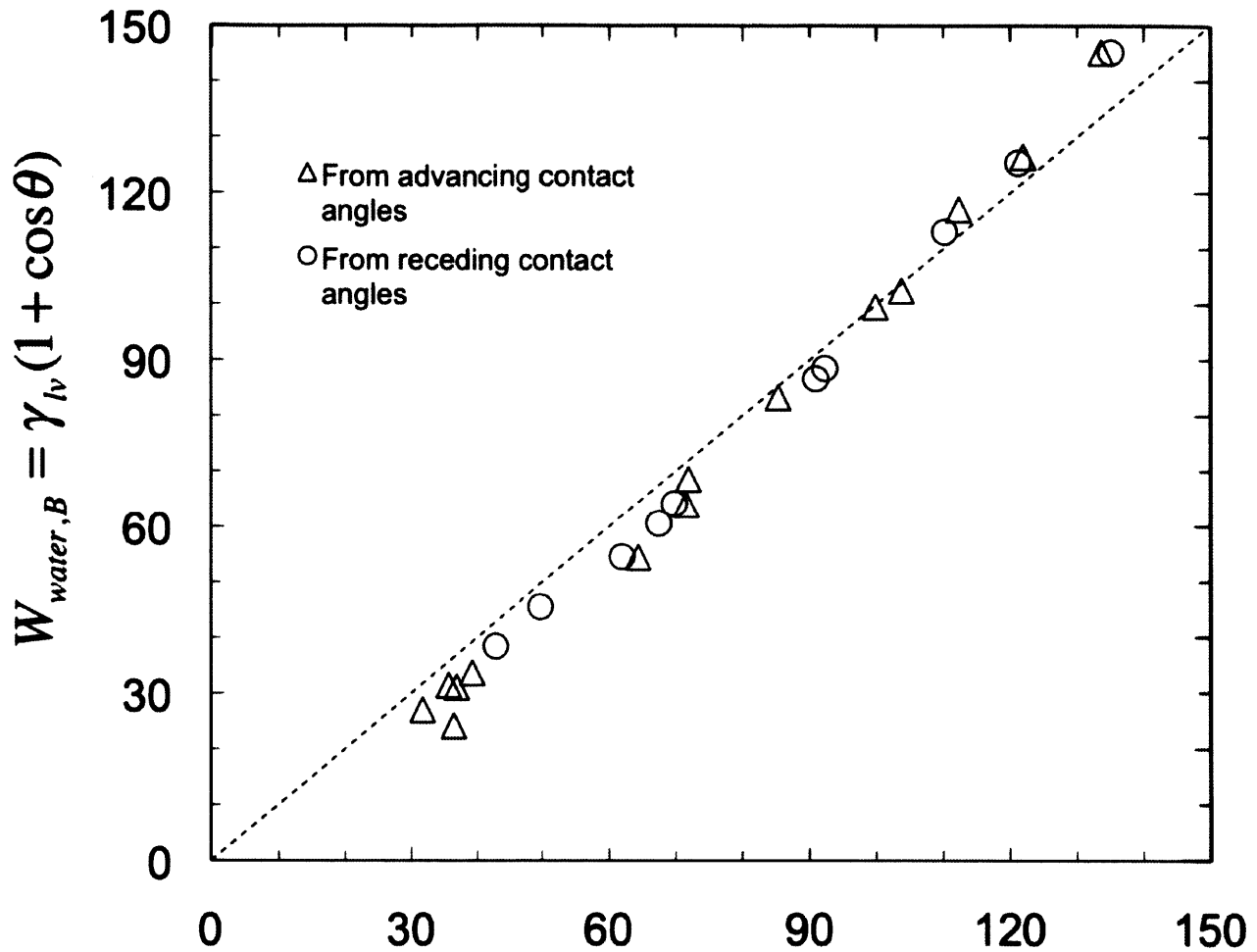
water[41].

Figure 5. Work of adhesion of liquid water calculated using measured advancing and receding contact angles are plotted against the work of adhesion of ice, calculated from advancing and receding surface energies.

Utilizing similar concept of approximating the work of adhesion of ice with the practical work of adhesion of liquid water in developing ice adhesion strength correlations, a probe fluid was selected to be used in estimating the work of adhesion of solid hydrate through receding contact angle measurements and Eq. 3. The 19.1 wt.% THF solution used to form hydrate was the natural choice. The practical work of adhesion of this solution, determined from

measurements of receding contact angles, was correlated with the measured adhesion strength of THF hydrate.

In Figure 6, THF hydrate adhesion strength is plotted against the normalized practical work of adhesion, $1 + \cos\theta_{rec}$, of the 19 wt. % THF solution, demonstrating a correlation between them. Thus, the practical work of adhesion of THF solution can be used to estimate the adhesion strength of THF hydrate. This correlation exists presumably because the polar and van der Waals surface energy properties of the 19.1 wt.% THF solution reflect those of THF hydrate, just as water reflects the surface energy properties of ice. The high surface energies of clean glass and steel result in their complete wetting by the THF/water solution (0° receding contact angle). For these surfaces the normalized work of adhesion may be greater than two ($1 + \cos(0)$). For this reason, these points were excluded from the correlation, while presented on the plot to demonstrate their much greater adhesion to hydrate compared to the treated substrates. The lowest hydrate adhesion strength was observed on the 80%/20% PEMA/fluorodecyl POSS treated steel disc, which exhibited the highest receding contact angle of the THF/water solution (90°). The positive slope and monotonic behavior of the data plotted in Figure 6 suggest that lower hydrate adhesion could be achieved on surfaces with lower practical work of adhesion to hydrates. This can be accomplished by tailoring the surface chemistry to minimize the polar and van der Waals interactions that govern Eq. 1. Although the PEMA/POSS blend tested in this work exhibits extremely low van der Waals interactions, and nearly zero polar interactions, some surfaces have been shown to exhibit net repulsive acid base interactions, that is, the acid-base interaction terms in Eq. 1 can be negative[42]. Thus, further reductions in adhesion strength on smooth surfaces may be possible.

To choose an appropriate fit for plotting adhesion strength of a solid (here THF hydrate) against the work of adhesion a probe fluid we first argue that the work of adhesion, W_{AB}^a, of any probe fluid (A) with non-zero, positive values of $\sqrt{\gamma_A^{LV}}$, $\sqrt{\gamma_A^+}$, and $\sqrt{\gamma_A^-}$ to a substrate (B) can be zero if and only if the adhesion strength of the solid itself on that substrate is zero. This is understood by studying Eq. 1, which is valid for both solids and liquids. For non-zero, positive surface energy parameters, $\sqrt{\gamma_A^{LV}}$, $\sqrt{\gamma_A^+}$, and $\sqrt{\gamma_A^-}$, of a probe fluid, $W_{AB}^a = 0$ implies that the surface energy parameters of the substrate material, $\sqrt{\gamma_B^{LV}}$, $\sqrt{\gamma_B^+}$, and $\sqrt{\gamma_B^-}$, must be zero. Consequently, the work of adhesion of the solid (here THF hydrate) to that substrate must be zero. The net adhesive force between two materials, resulting from van der Waals and Lewis acid-Lewis base interactions, decays monotonically with separation distance. Therefore, W_{AB}^a, which is the integrated dot product of net adhesive force and the separation distance, is zero if and only if the maximum force of separation is zero. It follows that the maximum stress (normal or shear), $\tau_{max,AB}$, required to separate THF hydrate from a surface is zero if and only if the work of adhesion to that substrate, W_{AB}^a, of any probe fluid having positive values of $\sqrt{\gamma_A^{LV}}$, $\sqrt{\gamma_A^+}$, and $\sqrt{\gamma_A^-}$ is zero. In conclusion, any physically meaningful fit to data relating adhesion strength of a material to the work of adhesion of any other material must pass through the origin.

The correlation between hydrate adhesion strength and the THF/water solution (Figure 6) is linear and passes through the origin ($R^2 = 0.90$), consistent with the fact that hydrate adhesion strength must approach zero as the work of adhesion of a probe fluid approaches zero. In comparison, if DI water is used as a probe fluid (Figure 7) a linear correlation passing through the origin is relatively poor ($R^2 = 0.51$). The improved fit attained by when hydrate adhesion

strength is plotted against the practical work of adhesion of the 19.1 wt% THF/water may be due

to the THF/water solution having surface energy properties closer those of the THF hydrate than

to those of water.

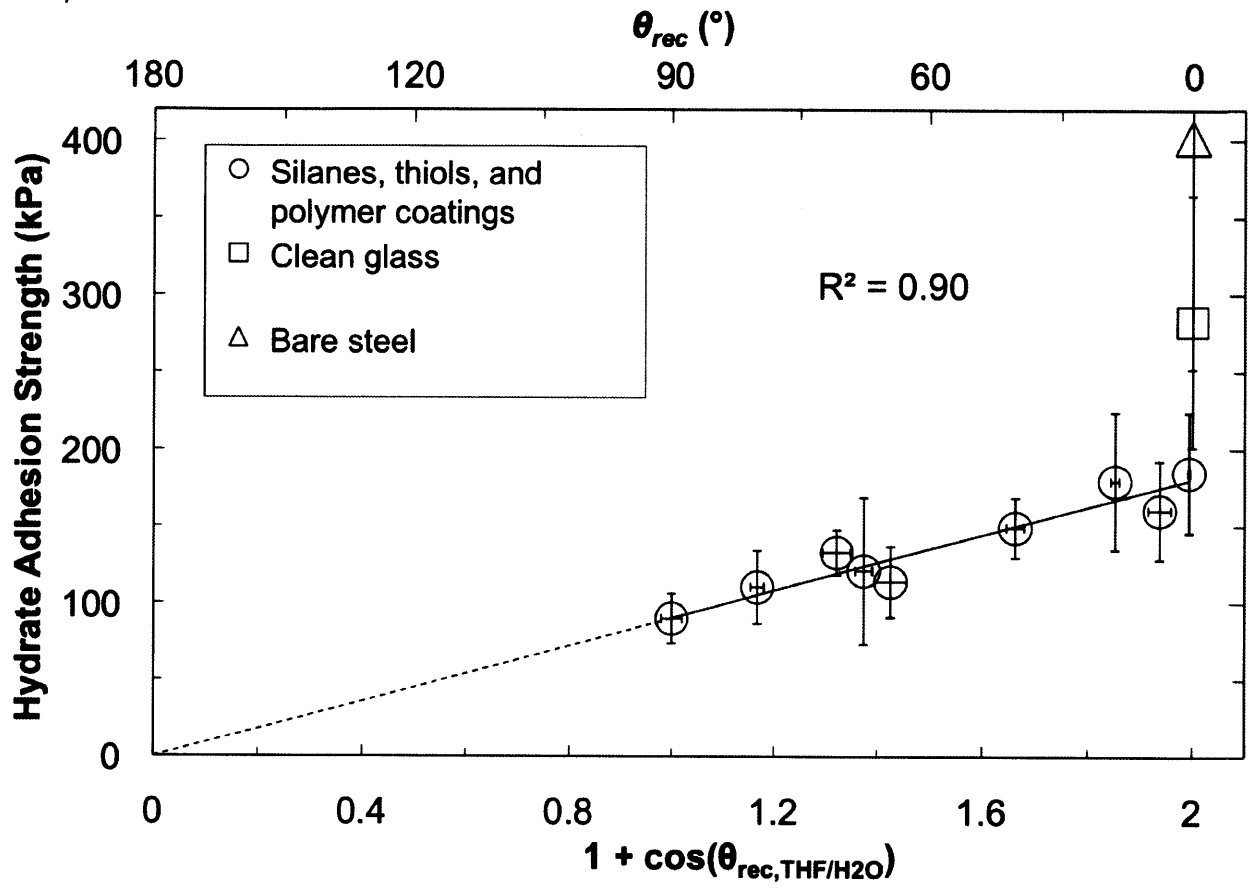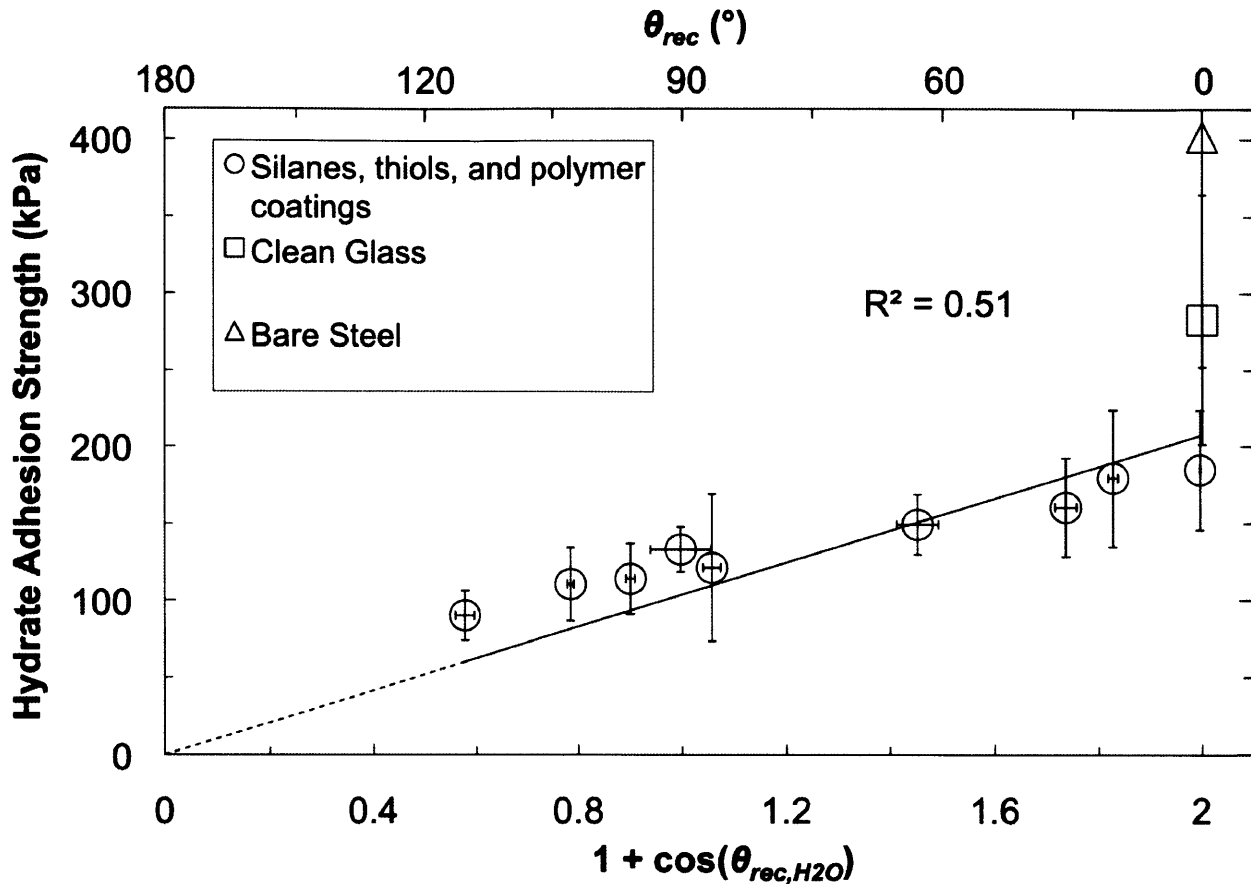**Figure 6.** Hydrate adhesion strength plotted against the practical work of the 19.1 wt.% THF/water solution.

Figure 7. Hydrate adhesion strength plotted against the practical work of adhesion of liquid water

Conclusions

More than a 75% reduction in adhesion strength of THF hydrate was demonstrated on treated surfaces compared with bare steel. This reduction is achievable on surfaces characterized by low Lewis acid, Lewis base, and van der Waals interactions, such that the work of adhesion (Eq. 1) is minimized. The thermodynamic work of adhesion between two solid materials cannot be easily measured in practice, and is therefore not a practical tool for predicting adhesion strength. However, hydrate adhesion strength was correlated with the practical work of adhesion, $\gamma(1 + \cos\theta_{rec})$, of a suitable probe fluid, that is, one with similar surface energy

properties to those of the hydrate. Therefore, practical work of adhesion measurements of a suitable probe fluid may serve as a valuable tool for predicting hydrate adhesion strength.

Unlike THF hydrate, a liquid with identical chemistry to a gas hydrate is unstable, as the solubility of a hydrate-stabilizing gas in liquid water is much lower than its concentration in the hydrate phase. Thus, the surface energies of gas hydrates, such as methane hydrate, must be measured using vOCG analysis, and a liquid solution designed with commensurate surface energy properties. This solution can then serve as a probe fluid to predict the adhesion strengths of gas hydrates to various materials, providing a much simpler alternative to high pressure gas hydrate adhesion testing. This approach can therefore lead to rapid screening of potential hydrate-phobic surfaces, such as those with specific chemistry chosen to minimize polar and van der Waals interactions governing the work of adhesion.

The expected trend beyond the range of the data acquired (labeled with a dashed line in Figure 6) suggests that further reductions in hydrate adhesion could be achieved by tailoring polar interactions to enhance repulsive polar interactions between the substrate and the hydrate. Hydrate adhesion may be further reduced by tailoring nano- and microscale surface morphology and chemistry to prevent penetration of the hydrate into the texture (as we have seen with ice [43]) such that the hydrate rests atop the texture features to reduce contact at the hydrate/substrate interface. This approach has already been successful for reducing ice adhesion on superhydrophobic surfaces [44-46] under conditions unfavorable to frost formation. Reduction of hydrate adhesion using textures will be the focus of future studies.

The results of this work suggest possible extension of the probe fluid approach to predicting adhesion strength between many other materials: the practical work of adhesion of a material in its liquid state to a substrate could be used to estimate the adhesion strength of the same material in its solid state to a substrate. The approach to predicting adhesion strength and methods of controlling adhesion strength laid out in this paper could benefit many industrial applications such as de-icing, welding, composite materials, thin films and coatings, and salt scaling.

As the world's energy demands are rapidly increasing, there is a strong shift towards the expansion of deep-sea drilling. Cheaper and more effective methods of gas hydrate mitigation must be found in order for this movement to be economical and safe. The principles discussed in this paper provide a framework for the development of hydrate-phobic surfaces, which in turn provides a pathway to passive enhancement of flow assurance and prevention of catastrophic failures in deep-sea oil and gas operations.

Bibliography

[1] *World Energy Outlook Homepage*. Available: http://www.worldenergyoutlook.com/

[2] E. Dendy Sloan and C. Ann Koh, "Clathrate hydrates of natural gases," 2008.

[3] E. D. Sloan Jr, "Fundamental principles and applications of natural gas hydrates," *Nature*.

[4] A. Sum, *et al.*, "Clathrate Hydrates: From Laboratory Science to Engineering Practice," *Industrial & Engineering Chemistry Research*.

[5] B. C. Gbaruko, *et al.*, "Gas hydrates and clathrates: Flow assurance, environmental and economic perspectives and the Nigerian liquified natural gas project," *Journal of Petroleum Science and Engineering*, vol. 56, pp. 192-198, 2007.

[6] C. A. Koh, *et al.*, "Mechanisms of gas hydrate formation and inhibition," *Fluid Phase Equilibria*, vol. 194-197, pp. 143-151, 2002.

[7] V. M. Bilyushov, "Mathematical model of hydrate formation in the flow of moist gas in tubes," *Journal of Engineering Physics and Thermophysics*, 1984.

[8] P. Bishnoi and V. Natarajan, "Formation and decomposition of gas hydrates," *Fluid Phase Equilibria*, vol. 117, pp. 168-177, 1996.

[9] D. Kashchiev and A. Firoozabadi, "Driving force for crystallization of gas hydrates," *Journal of Crystal Growth*, vol. 241, pp. 220-230, 2002.

[10] D. Kashchiev and A. Firoozabadi, "Nucleation of gas hydrates," *Journal of Crystal Growth*, vol. 243, pp. 476-489, 2002.

[11] M. Anklam and A. Firoozabadi, "Driving force and composition for multicomponent gas hydrate nucleation from supersaturated aqueous solutions," *The Journal of Chemical Physics*, vol. 121, pp. 11867-11867, 2004.

[12] B. J. Anderson, *et al.*, "Properties of inhibitors of methane hydrate formation via molecular dynamics simulations," *J. Am. Chem. Soc*, vol. 127, pp. 17852-17862, 2005.

[13] S. R. Davies, *et al.*, "Studies of hydrate nucleation with high pressure differential scanning calorimetry," *Chemical Engineering Science*, 2009.

[14] M. Walsh, *et al.*, "Microsecond Simulations of Spontaneous Methane Hydrate Nucleation and Growth," *Science*, vol. 326, pp. 1095-1098, 2009.

[15] T. Koga, *et al.*, "Hydrate Formation at the Methane/Water Interface on the Molecular Scale," *Langmuir*, vol. 26, pp. 4627-4630, 2010.

[16] S.-o. Yang, *et al.*, "Temperature dependence of particle-particle adherence forces in ice and clathrate hydrates," *Journal of Colloid and Interface Science*, vol. 277, pp. 335-341, 2004.

[17] C. Taylor, *et al.*, "Micromechanical adhesion force measurements between tetrahydrofuran hydrate particles," *Journal of Colloid and Interface Science*, vol. 306, pp. 255-261, 2007.

[18] C. J. Taylor, *et al.*, "Hydrate Particles Adhesion Force Measurements: Effects Of Temperature, Low Dosage Inhibitors, and Interfacial Energy," 2008.

[19] L. E. Dieker, *et al.*, "Micromechanical Adhesion Force Measurements between Hydrate Particles in Hydrocarbon Oils and Their Modifications," *Energy & Fuels*, vol. 23, pp. 5966-5971, 2009.

[20] J. W. Nicholas, *et al.*, "Assessing the feasibility of hydrate deposition on pipeline walls--Adhesion force measurements of clathrate hydrate particles on carbon steel," *Journal of Colloid and Interface Science*, vol. 331, pp. 322-328, 2009.

[21] G. Aspenes, *et al.*, "Adhesion force between cyclopentane hydrates and solid surface materials," *Journal of Colloid and Interface Science*, 2009.

[22]A. J. Meuler, *et al.*, "Relationships between Water Wettability and Ice Adhesion," *ACS Applied Materials & Interfaces*, vol. 2, pp. 3100-3110, 2010.

[23]V. F. Petrenko and R. W. Whitworth, "Physics of ice," pp. 373-373, 1999.

[24]A. J. Meuler, *et al.*, "Relationships between Water Wettability and Ice Adhesion," *ACS Applied Materials & Interfaces*, 2010.

[25]J. Mabry, *et al.*, "Fluorinated Polyhedral Oligomeric Silsesquioxanes (F-POSS)," *Angewandte Chemie*, vol. 120, pp. 4205-4208, 2008.

[26]R. J. Good, "Contact angle, wetting, and adhesion: a critical review," *Journal of Adhesion Science and Technology*, vol. 6, pp. 1269-1302, 1992.

[27]E. Cortes, *et al.*, "Enhanced Stability of Thiolate Self-Assembled Monolayers (SAMs) on Nanostructured Gold Substrates," *Langmuir*, vol. 25, pp. 5661-5666, 2009.

[28]M. Strobel and C. S. Lyons, "An Essay on Contact Angle Measurements," *Plasma Processes and Polymers*.

[29]F. Garbassi, *et al.*, *Polymer surfaces from physics to technology*: Wiley, 1994.

[30]Y. Uyama, *et al.*, "Comparison of different methods for contact angle measurement," *Journal of Colloid and Interface Science*, vol. 141, pp. 275-279, 1991.

[31]L. M. Lander, *et al.*, "A systematic comparison of contact angle methods," *Langmuir*, vol. 9, pp. 2237-2239, 1993.

[32]C. E. Stauffer, "The Measurement of Surface Tension by the Pendant Drop Technique," *The Journal of Physical Chemistry*, vol. 69, pp. 1933-1938, 1965.

[33]R. N. Wenzel, "Resistance of Solid Surfaces to Wetting by Water," *Industrial & Engineering Chemistry*, vol. 28, pp. 988-994, 1936.

[34]C. J. Van Oss, *et al.*, "Interfacial Lifshitz-van der Waals and polar interactions in macroscopic systems," *Chemical Reviews*, vol. 88, pp. 927-941, 1988.

[35]D. H. Bangham and R. I. Razouk, "Adsorption and the wettability of solid surfaces," *Transactions of the Faraday Society*, vol. 33, pp. 1459-1463, 1937.

[36]A. A. Griffith, "The Phenomena of Rupture and Flow in Solids," *Philosophical Transactions of the Royal Society of London. Series A, Containing Papers of a Mathematical or Physical Character*, vol. 221, pp. 163-198, January 1, 1921 1921.

[37]S. J. Bennett, *et al.*, "Adhesive fracture mechanics," *International Journal of Fracture*, vol. 10, pp. 33-43, 1974.

[38]D. Maugis and M. Barquins, "Fracture mechanics and the adherence of viscoelastic bodies," *Journal of Physics D: Applied Physics*, vol. 11, pp. 1989-1989, 1978.

[39]A. A. Volinsky, *et al.*, "Interfacial toughness measurements for thin films on substrates," *Acta Materialia*, vol. 50, pp. 441-466, 2002.

[40]C. J. Van Oss, *et al.*, "Surface tension parameters of ice obtained from contact angle data and from positive and negative particle adhesion to advancing freezing fronts," *Journal of Adhesion Science and Technology*, vol. 6, pp. 503-516, 1992.

[41]K. L. Mittal, "Adhesion Measurement of Thin Films, Thick Films and Bulk Coatings," *ASTM Special Technical Publication*, vol. 640, pp. 5-16, 1976.

[42]K. L. Mittal, "Acid-base interactions: relevance to adhesion science and technology" p. 380, 1991.

[43]K. K. Varanasi, *et al.*, "Frost formation and ice adhesion on superhydrophobic surfaces," *Applied Physics Letters*, vol. 97, pp. 234102-234102, 2010.

[44]F. Dotan, *et al.*, "The Relationship between Water Wetting and Ice Adhesion," *Journal of Adhesion Science and Technology*, vol. 23, pp. 1907-1915, 2009.

[45] S. A. Kulinich and M. Farzaneh, "Ice adhesion on super-hydrophobic surfaces," *Applied Surface Science,* vol. 255, pp. 8153-8157, 2009.

[46] S. A. Kulinich and M. Farzaneh, "How Wetting Hysteresis Influences Ice Adhesion Strength on Superhydrophobic Surfaces," *Langmuir,* vol. 25, pp. 8854-8856, 2009.